Crucial roles of phase competition and spin-lattice relaxation in the gigantic switchable optomagnet effect of $(Fe_{0.875}Zn_{0.125})_2Mo_3O_8$

Y. H. Zhuang,[1] H. W. Liu,[1] Y. H. Li,[1] Y. M. Chang,[2] T. Kurumaji [3] Y. Tokura [4,5,6] and Y. M. Sheu [1,7,*]

[1]*Department of Electrophysics, National Yang Ming Chiao Tung University, Hsinchu 30010, Taiwan*
[2]*Department of Electrophysics, National Chiao Tung University, Hsinchu 30010, Taiwan*
[3]*Department of Advanced Materials Science, University of Tokyo, Kashiwa 277-8561, Japan*
[4]*RIKEN Center for Emergent Matter Science, Wako, Saitama 351-0198, Japan*
[5]*Department of Applied Physics and Quantum Phase Electronics Center, University of Tokyo, Bunkyo-ku, Tokyo 113-8656, Japan*
[6]*Tokyo College, The University of Tokyo, Tokyo 113-8656, Japan*
[7]*Center for Emergent Functional Matter Science, National Yang Ming Chiao Tung University, Hsinchu 30010, Taiwan*

It was discovered that crystal-field excitations involving spin-flip transitions play a crucial role in controlling switchable optomagnet effects in antiferromagnetic $(Fe_{0.875}Zn_{0.125})_2Mo_3O_8$. However, when the flipped spins are in excited states to frustrate the balanced spin moments, the photoinduced magnetization has not occurred yet. Only after the ultrashort pulses disappear does the gigantic magnetization start to grow from a zero moment. In this study, we demonstrate that the gigantic optomagnetic effect is triggered by a two-step spin-flip process. Through the use of Kerr-effect microscopy and applications of the magnetic field, we discern between photoinduced switchable magnetization and nonswitchable demagnetization. Our experimental designs uncover all indispensable factors for the development of antiferromagnetic memory devices using insulating oxides.

I. INTRODUCTION

In the past, the majority of studies on light-induced ultrafast magnetism focused on demagnetization processes from nonzero moments in various ferro or ferrimagnetic systems [1–20]. Magnetization from a zero moment in antiferromagnets was relatively less explored [21,22]. In the first case, the application of magnetic fields was typically required, whereas the later case did not necessitate external fields. Exceptional cases involved coherent control [23–28] or optical THz excitation [29–34], which manipulated spin wave or magnons via various well-established mechanisms [35,36], either far away from resonance or at near resonance, respectively. In contrast to the prevalent use of the NIR-field (mostly at 800 nm) or the THz-field excitation, crystal-field excitation has been rarely employed in ultrafast (de)magnetization [22,37]. In transition metal oxides, crystal-field splitting induced from effective fields created by surrounding oxygens enables on-site d-d transitions due to the lifting degeneracy of d orbitals. Recent breakthroughs have been discovered through such on-site d-d transitions, offering a new route for switchable antiferromagnetic spintronics [22] and providing critical nonreciprocity [38] for isolator device applications.

When spin subsystem change is discussed in the nonequilibrium case after photoexcitation, the three temperature model is often adopted in magnetic metals [1] while a picture of excess energy transfer is mostly used in magnetic insulators for above-gap excitations [39]. Although the on-site spin flip can be realized by crystal-field excitations that induce transient change in spin arrangements, excited state lifetimes, electron correlations, and the following thermal dynamics together make it hard to predict magnetization change straightforwardly. It is also unknown whether the excited state emits a magnon and then precesses to a different state or back to a ground state. Undoubtedly, crystal-field excitation plays a key role in switchable optomagnet effects for antiferromagnetic materials. However, the interplay remains unclear as to the excited spin-state lifetime, the following relaxation, and the spontaneous magnetization after the disappearance of pulse excitation. To reveal all essential pivots, we design the experiment to compare the wave vector of crystal-field excitation perpendicular to $(k_\perp)$ and parallel to $(k_\parallel)$ the Néel vector. We also employ scanning Kerr microscopy and magnetic field to compare the role of the antiferromagnetic and ferrimagnetic state in a switchable optomagnetic material of strong phase competition. These experimental designs demonstrate a two-step spin-flip process for enhancing the optomagnetic effect and distinctively elucidate differences between switchable ultrafast magnetization versus nonswitchable ultrafast demagnetization, providing deeper insight into ultrafast magnetism.

II. SAMPLE AND EXPERIMENT SETUP

Figures 1(a) and 1(b) show the crystal and magnetic structures of $Fe_2Mo_3O_8$(FMO). The magnetic ions, Fe^{2+}, are located in oxygen octahedrons (O-site) and tetrahedrons (T-site), and have alternative stacking along the c axis with nonmagnetic Mo^{4+} in oxygen octahedrons.
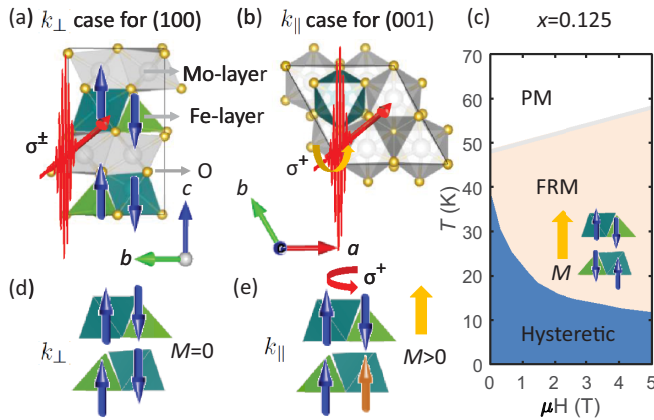
*ymsheu@nycu.edu.tw

024421-1

FIG. 1. Illustrations of experimental geometries for (a) (100) and (b) (001) $(Fe_{1-x}Zn_x)_2Mo_3O_8$, corresponding to $k_\perp$ and $k_\parallel$, respectively. (c) A phase diagram for $x = 0.125$, adopted from Ref. [40] where the phase and phase boundary were determined by M-T or M-H curves. The AFM (FRM) state occurs in the hysteresis region without (with) field cooling. (d) In the $k_\perp$ geometry, a circularly polarized pump excites both O-site spins in a magnetic unit of AFM order. (e) A circularly polarized pump only selectively flips spin moments in the $k_\parallel$ geometry.

When nonmagnetic Zn replaces Fe at the T-site, i.e., $(Fe_{1-x}Zn_x)_2Mo_3O_8$(FZMOx), FZMOx exhibits an antiferromagnetic (AFM) ground state and experiences increasing phase competition with a ferrimagnetic (FRM) phase [39]. Figure 1(c) presents a phase diagram for $x = 0.125$, which exhibits the strongest phase competition and the largest hysteretic area among various doping concentrations [39]. Additionally, the optomagnetic effect, which creates switchable transient magnetization from zero magnetic moment in the AFM ground state by using crystal-field excitation to selectively excite d-d transitions from one of the four Fe^{2+} ions in a magnetic unit displayed in Fig. 1(d) is maximized in this doping concentration [22]. The application of magnetic fields can stabilize the FRM phase, as shown in the magnetic structure displayed in Fig. 1(c). For a comprehensive discussion of the material properties, refer to Ref. [39], while Ref. [22] provides in-depth analysis on the optomagnetic effect.

Our experiments utilize a 1.24-eV pump and a 0.87-eV probe generated by an amplifier laser centered at 1030 nm with a pulse width of $\sim$200 fs and a repetition rate of 5 kHz. The crystal-field excitation at 1.24 eV enables on-site spin-flip d-d transition of Fe^{2+} located at O-sites [22]. In the $k_\perp$ configuration [Fig. 1(a) and 1(d)], circularly polarized light has the same probability to excite both up and down spin along the crystal c-axis (as illustrated in Fig. 5(a) in Appendix A); thus, we opt for linearly polarized pump in the $k_\perp$ case. However, in the $k_\parallel$ configuration [Fig. 1(b) and 1(e)], the light helicity selects either up or down spin solely, effectively frustrating the antiferromagnetism during pulse irradiations and enabling the generation of optomagnetic effects [see Fig. 5(b) in Appendix A]. Hence, we use circularly polarized light (σ^-) in this case. In the $k_\perp$ case, we measure the magnetooptical anisotropy arising from magnetic linear birefringence in the ac plane, which is characterized by different reflectance (ΔR) for light polarization parallel to ($E \parallel$) or perpendicular to

($E \perp$) Néel vector $[\Delta R_{ac}(t) = R_\perp(t) - R_\parallel(t)]$. In the $k_\parallel$ case, we measure polar Kerr rotations (θ) originating from magnetic circular birefringence $[\Delta\theta(t) \propto \Delta M(t)]$. Apart from the probe polarizations, both excitation geometries share the same pump-probe setup. In the $k_\perp$ case, our probe light is polarized at 45° relative to the Néel vector to measure the maximum magnetooptical anisotropy. Since the Kerr rotation signal is independent of probe polarizations, the S-polarized probe is utilized in the $k_\parallel$ case. The majority of experiments are performed without field cooling to reach the AFM state and with low excitation fluence of around 0.4 mJ/cm² to minimize optical anisotropy arising from crystal anisotropy (due to crystal birefringence) in the $k_\perp$ case, unless otherwise stated.

III. DISCUSSION

Figure 2(a) displays the time-resolved magnetooptical Kerr rotations corresponding to the optomagnetic effect at various temperatures. The signal gradually increases and reaches a maximum around 45 K before it decreases and nearly disappears above 48 K [T_c for $x = 0.125$ as in Fig. 1(c)]. Similar signal evolution with temperature rise also occurs for $x = 0.25$, and the signal reaches maximum at around 30 K before it nearly disappears at 40 K (T_c for $x = 0.25$). For pure FRM phase in the magnetic ordered state, e.g., $x = 0.4$, such temperature evolution and the Kerr rotation enhancement completely vanish [22]. While M-H and M-T measurements may suggest FRM as a ground state between 37 to 48 K [Fig. 1(c)] and AFM metastable state below 37 K for $x = 0.125$, Fig. 1(c), our Kerr rotation signal implies the AFM state still coexisting with FRM. Accompanying the fact that the pure FRM state in $x = 0.4$ does not display any enhancement may further imply a possibility of AFM being a ground state for $\mu H = 0$ below T_c.

A complementary support for the above suggestion can be found in our confocal-scanning-Kerr-microscopic images, Fig. 2(b), which measures the competing FRM domain. The FRM image for $x = 0.125$ does not have discernible change below 44 K. Figure 2(c) displays intensity distributions for all pixels of the individual image. It even reveals a slight decrease in the contrast at 43 K, at which the FRM was supposed to be the ground state that showed a regular hysteresis curve [39], yet our Kerr rotation signal is approaching a maximum change [Fig. 2(a)]. A similar result happens for $x = 0.25$ below 35 K, see Fig. 6 in Appendix B. Clearly, the image indicates that, without magnetic fields applied, the FRM state does not grow to increase the domain contrast due to more AFM changing to the FRM phase, nor does the domain size vary due to the increase of dipole-dipole interactions upon temperature rise [41]. These results point to the fact that the coexisting AFM phase remains below T_c, but its free-energy barrier to the FRM phase continues to decrease or become comparable upon temperature rise. The combination of spatially and temporally resolved measurements clearly unveil the sophisticated phase competition that cannot be anticipated solely by a static measurement.

The above discussion points to the indispensability of the AFM state and phase competition, without either of which the enormously switchable optomagnetic effect will not occur. For FZMOx, Zn doping reduces intralayer coupling $J_{\perp c}$ and
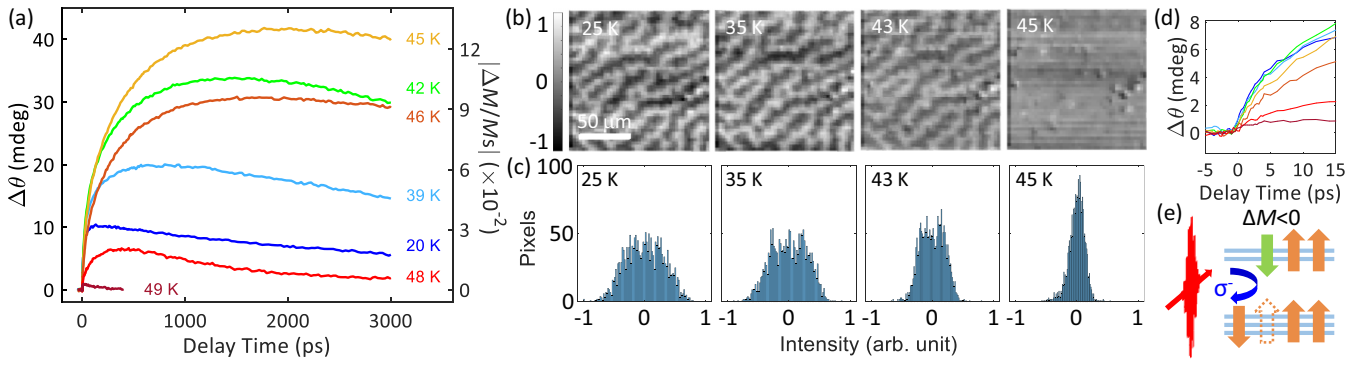
FIG. 2. (a) Temperature-dependent Kerr rotation angles and the corresponding magnetization measured with pump of σ^- polarization in the $k_\parallel$ geometry. (b) Images obtained from a confocal scanning Kerr microscopy at 25, 35, 43, and 45 K. The horizontal lines in the 45-K image are artifacts due to mechanically scanning direction, rotating which with 90 degree results in vertical artifacts. The domain image disappears at 45 K because of the accumulated heating effect from using a high-repetition-rate laser oscillator, while no such effect occurs in (a) due to the employment of a low-repetition-rate laser amplifier. (c) The corresponding statistics of (b). The contrast distribution becomes narrower and sharper at 45 K due to the disappearance of the domain. (d) The zoom-in of (a) around zero time delay. (e) The illustration of crystal-field excitation from the O-site with σ^- used in (a).

interlayer T-site coupling J_{tt}, enhancing the AFM and FRM phase competition [22]. Only when 40% Zn replaces Fe at the T-site does the magnetic ground state become FRM, losing the competing AFM phase and gigantic optomagnetic effect. While both doping and the photoinduced changes in exchange interaction all favor the excited spin state [22], clearly, the initial slow rise of Kerr rotation, corresponding to spontaneous magnetization after pulse disappearance [Fig. 2(d)], seems to imply weak relevance to the magnetization directly associated with the excited spin state [Fig. 2(e)].

To identify an origin of the spontaneous magnetization after the disappearance of the 200-fs pulse, we compare the time-resolved Kerr rotation and magnetooptical anisotropy at different temperatures for $k_\parallel$ [Fig. 2(a)] and $k_\perp$ [upper panel of Fig. 3(a)], respectively. We see that the signal nearly disappears for both measurements above the transition temperature of 48 K, indicating direct probes of magnetic order parameters. Since the optical anisotropy has eliminated any isotropic signals, it leaves magnetic anisotropy as the origin, i.e., along or perpendicular to the Néel vector. If we zoom-in to further compare the two measurements before 1 ps, Figs. 2(d) and 3(b), we see a clear pulse-like feature in magnetooptical anisotropy for $k_\perp$ while it never occurs in Kerr rotation for $k_\parallel$. After the pulse-like feature and before 500 ps, the magnetooptical anisotropy grows slowly. This pulse-like feature matches the timescale of our autocorrelation signal arising from pump and probe pulses being spatially and temporally overlapped on the crystal, Fig. 3(b). There is no commonly observed electron-phonon coupling time on a timescale of 1 ps, Fig. 3(a).

As low excitation in optical anisotropy is prevailed by magnetic origin, to verify the lattice heating time we increase pump fluence at a temperature above T_c, leading to dominating crystal anisotropy from lattice heating. The lower panel in Fig. 3(a) displays crystal anisotropy for various fluence and a pulse correlation signal is overlapped at zero delay time. We first can see a linear dependence of crystal anisotropy versus pump fluence, indicating pure lattice heating in the signal without other contributions. Now we pay attention to signals

near zero time delay and we can unambiguously see that the maximum crystal anisotropy immediately occurs after the
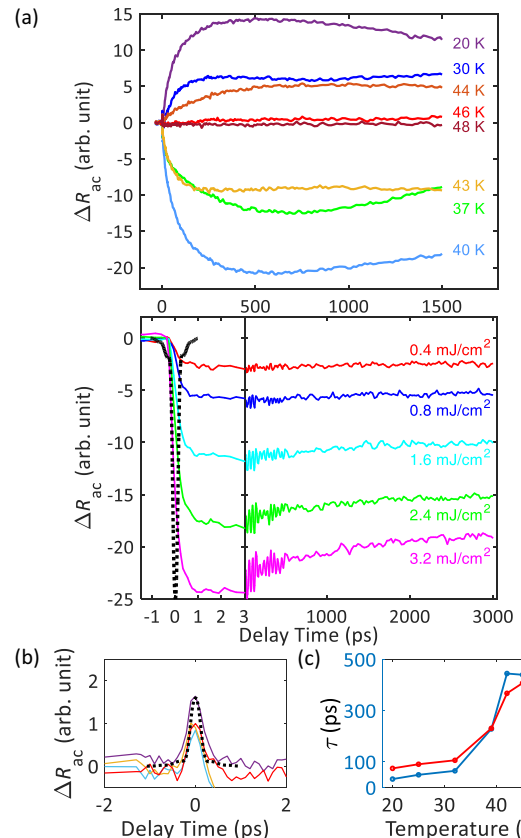

FIG. 3. (a) Optical anisotropy of ac plane measured from $k_\perp$ geometry at various temperatures (upper panel) and with various pump fluence at 60 K (lower panel). The sign change is beyond the scope of this article and the interpretation is provided in the Appendix C. (b) The zoom in of the upper panel of (a). The black dotted lines in lower panel of (a) and in (b) depict intensity autocorrelations of our pulsed laser. (c) Temperature evolution of two rising times were derived from exponential fittings of Kerr rotations in Fig. 2(a).

pulse correlation. This is clear evidence that the major lattice heating has already occurred during the pulse excitation. No additional electron-phonon coupling time is found here. This is a disparate behavior compared to the above-gap excitation for insulators where electron-phonon coupling can still take place due to the nature of conductive electrons above a gap. Here, localized electrons excited via crystal-field transition possess no conductive electron to scatter with phonon. When they return to the ground state, the energy is transferred to local sites, i.e., O-sites here when 1.24 eV is employed.

Since the excited flipping-spin mostly returns to the ground state within the pulse width, this step is not directly responsible for the gigantic magnetization after the disappearance of pulses, Fig. 2(a). Instead, the role of the excited flipping-spin plays is to change the nearby exchange coupling, i.e., enhance both the interlayer AFM coupling between the O- and T-sites ($J_\parallel$) and interlayer ferromagnetic coupling between the O-site (J_{OO}), as discussed in Ref. [22], that sets the favorable spin orientation determined from the pump light helicity. Figure 3(a) displays growths of magnetic anisotropy with the timescale becoming slower when the elevated temperature approaches T_c, consistent with the rising time observed in the Kerr rotation of Fig. 2(a). The rising time for the Kerr rotation signal can be fitted with two exponentials [42], Fig. 3(c), both showing a divergent behavior near T_c. Such dynamical slowing down for magnetic ordering, with or without spin flipping, is in line with the spin-lattice relaxation of material with a second-order phase transition [43].

All of the above discussion points out an essential fact that the relatively slow spin thermal dynamical properties can be controlled by ultrashort pulses without magnetic field applied. Indeed, while magnetic field applications can select a ferrimagnetic state, it suppresses the AFM state and the associated phase competition. Figure 4(a) exhibits pure demagnetization for three different pump polarizations after the sample cooled under a magnetic field pointing to sample normal (+c), Fig. 4(b). The resulting difference between pump polarizations comes from the degree of demagnetization due to various absorption, i.e., the absorption and demagnetization is minimized when the magnetization direction created by light helicities is the same as magnetic fields Fig. 4(b). Therefore, the pure FRM phase achieved by either doping or magnetic field merely leads to the destruction of the gigantic optomagnetic effect. Furthermore, despite the fact that, although helicity-induced contrast variations exist for both the optomagnetic effect in the AFM state and for ultrafast demagnetization in the single-phase and single-domain FRM state, the resulting macroscopic moments are fundamentally different—the first is a switchable ultrafast magnetization, while the second only involves different degrees of demagnetization.

Now we can depict a clear picture of using crystal-field excitation to create huge optomagnetic effects in chronological order. Figure 4(c) illustrates flipped spin instantaneously created upon an excitation of the circularly polarized pulse. This initial spin-flip process, referred to as the first flip shown in Fig. 4(c), occurs within a timescale of ∼0.4 ps, near the end of pump-probe correlation. At this point, the majority of the excited spin has relaxed to the ground state, transferring laser energies directly to the local excitation site, while a small
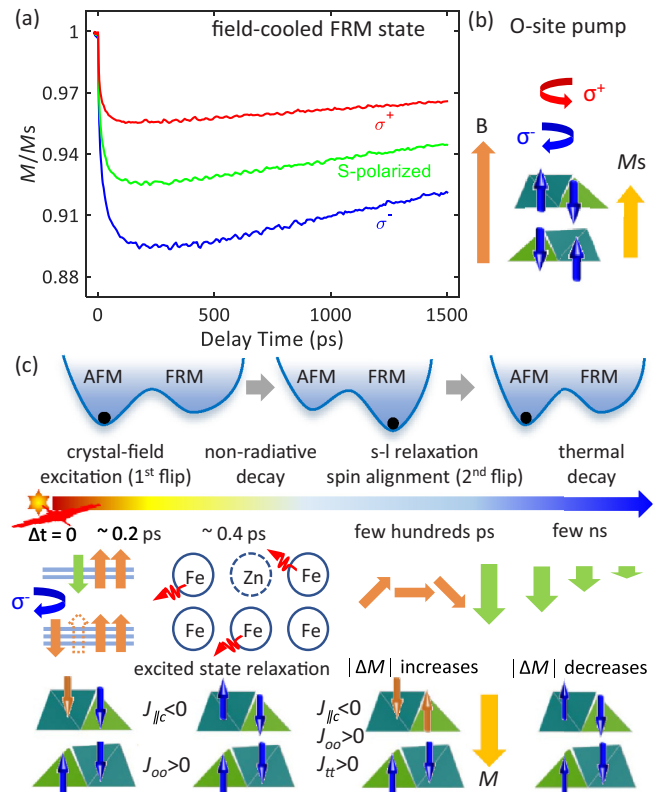

FIG. 4. (a) Magnetic signals measured from three different polarized pumps after the sample is field-cooled to a FRM state with 0.1 T. The signals are derived from Kerr rotations and then normalized by the saturated magnetization M_s induced from magnetic field B along the +c-axis (details can be found in Appendix D) as illustrated in (b), which also displays spin arrangements after our field cooling. (c) The illustration of timescale for the optomagnet effect after crystal-field excitations. The upper figure is instantaneous free-energy landscapes depicting evolutions of the barrier height between the AFM and FRM states. The lower figure is the spin excited state, its relaxation, the following spontaneous magnetization during spin-lattice relaxation, and the demagnetization during thermal decay. The difference of spin arrangements and transient exchange interactions for the first and the second flips are indicated in the lowest panel. See text for an in-depth discussion.

fraction retains in altered exchange interactions, serving as the trigger for the second-step spin flip [second flip shown in Fig. 4(c)] during the subsequent spin-lattice relaxation. This relaxation process occurs over a time constant ranging from tens of picoseconds to subnanoseconds, as depicted in Fig. 3(c). Throughout this process, the free-energy landscape of the competing AFM and FRM order undergoes changes. The reduction of the AFM-to-FRM barrier is determined from the elevated quasiequilibrium temperature. Therefore, at higher base temperatures of the sample, with the same excitation fluence, the induced magnetization becomes higher, as shown in Fig. 2(a). Although the spin-flip transition plays a direct role, there is no coherent magnetic precession observed in either Kerr rotation or magnetooptical anisotropy. This absence can be attributed to the fact that the spontaneous magnetization is thermodynamically driven by the competition between AFM and FRM phases during the spin-lattice

relaxation. As a result, the presence of the FRM ground state (double-well potential with lower free energy for the FRM phase) or a pure FRM phase (single-well potential) will not induce a substantial and robust optomagnetic effect during spin-lattice relaxation.

IV. CONCLUSION

In summary, while crystal-field excitation and polar structure are both critical to initiate a switchable spin-flipping transition, their roles are to enhance exchange couplings that are preferable for ferrimagnetic ordering upon pulse excitation. By employing different light propagation vectors in the experiments, we are able to infer the two-step spin-flip process that leads to the generation of the gigantic Kerr rotation. Additionally, the presence of spin-lattice relaxation and the coexistence of the AFM phase with a competing FRM phase are essential in creating enormous optomagnetic effects. The free-energy barrier for the FRM is either slightly higher (a few meV) or comparable to the AFM phase. However, reversing the order in the free-energy landscape or having a single FRM phase, whether field-trained or not, all exterminate the robustness of the spontaneous growth of the giant magnetic moment that is switchable by light helicity.

APPENDIX A: COMPARISON OF PUMP POLARIZATION IN TWO GEOMETRIES FOR $X = 0.125$

In the case of measuring ac plane optical anisotropy ($k_\perp$ case), the circularly polarized light has no spin selection. This argument is supported by our Fig. 5(a) where magnetooptical anisotropy exhibits nearly identical signals for three different light polarizations. In contrast, for the $k_\parallel$ case, where we measure Kerr rotation signals and their dependence on pump polarizations, as shown in Fig. 5(b), the signals exhibit polarity changes under different circularly polarized pumps, while a linearly polarized pump does not induce any significant signal. This observation implies the presence of opposite magnetic moments induced by light helicities from a zero moment state. The optomagnetic effect and the corresponding discussion can be found in Ref. [22].
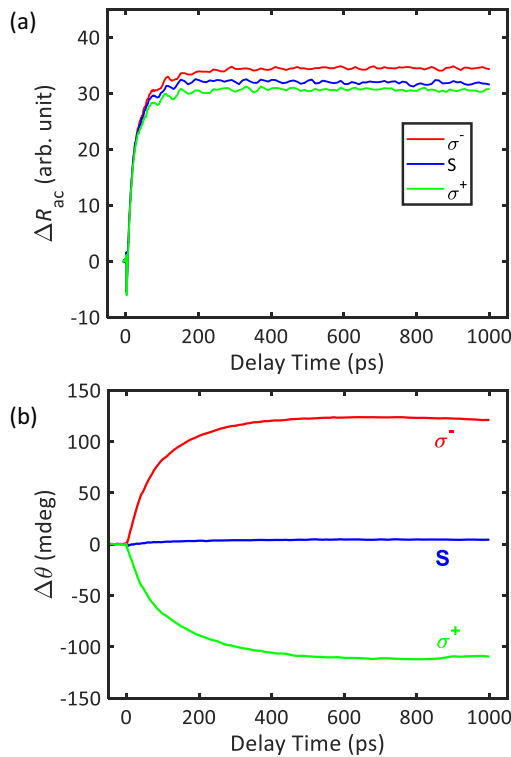

FIG. 5. (a) Magnetooptical anisotropy of ac plane in the $k_\perp$ case and (b) Kerr rotation signals of ab plane in the $k_\parallel$ case. Both cases are measured using different light polarizations from the $x = 0.125$ sample in the antiferromagnetic (AFM) state at 20 K.
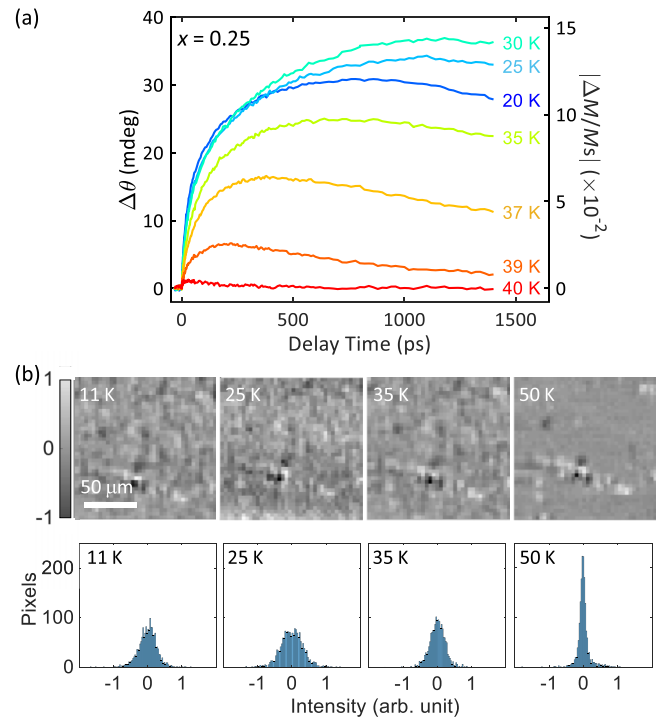

FIG. 6. (a) Temperature-dependent Kerr rotation angles and the corresponding magnetization measured for the sample with $x = 0.25$ in the $k_\parallel$ case using a circularly polarized pump (σ^-) of 0.4 mJ/cm^2. (b) The upper panel shows images obtained from confocal scanning Kerr microscopies of $x = 0.25$ at temperatures of 11, 25, 35, and 50 K. The color bar presents a scale for the surface without defects. In the lower panel, the corresponding contrast distributions are displayed, which are derived from statistics of the individual image.
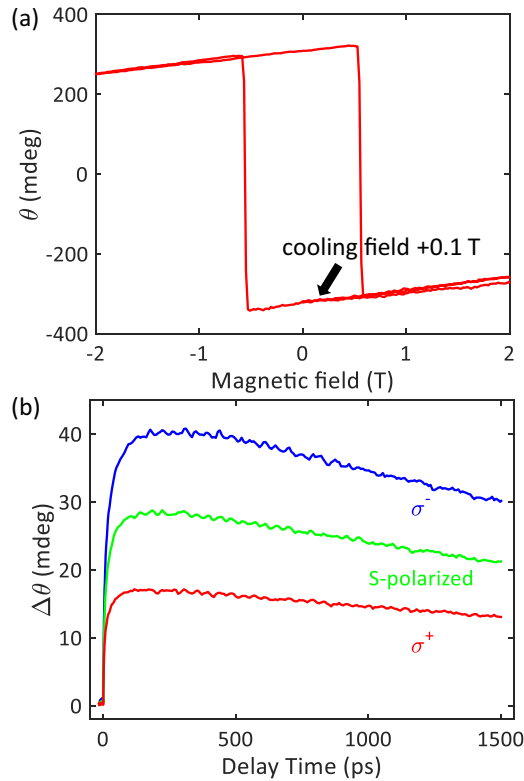
FIG. 7. (a) The hysteresis curve of $x = 0.125$ FZMOx obtained by Kerr rotation measurements at 20 K. (b) The change in Kerr rotations for different pump polarizations is depicted. The measurements are obtained after cooling the sample with a magnetic field along the $+c$ axis to achieve the FRM state. The arrow in (a) indicates the polarity of static Kerr rotation under our cooling field of 0.1 T.

APPENDIX B: SUPPORTING FIGURES FROM $X = 0.25$

A complementary figure illustrating a coexisting antiferromagnetic (AFM) state resulting from a Zn doping concentration of 25% ($x = 0.25$) is shown in Fig. 6(a). The maximum optomagnetic effect is observed at 30 K with enhancement still occurring below 40 K. Above this temperature, the material is in a paramagnetic state, while below it, *M*-*T* and *M*-*H* measurements determine this doping concentration as a ferrimagnetic (FRM) state.

Supporting figures for the coexistence of AFM in $x = 0.25$ are displayed in Fig. 6(b). There is no discernible change

in FRM domain images, including domain size and domain contrast below 40 K. The result is consistent with that of $x = 0.125$, except for the fact that the domain size is significantly reduced in the case of 25% doping concentration when the sample is not field-cooled prior to measurements.

APPENDIX C: INTERPRETATIONS FOR THE SIGN CHANGE IN THE TEMPERATUR-DEPENDENT OPTICAL ANISOTROPY

We observe two sign changes in Fig. 3(a) which occur between 30 to 38 K and between 43 and 46 K, respectively. The first one takes place near the boundary between the hysteretic/FRM phase, and the second one occurs near the FRM/PM phase boundary. When considering the significant growth of optomagnetic effects observed from Kerr rotations in Fig. 2(a) above 35 K until 45 K, followed by a decrease, it is highly likely that these changes are attributed to the increasing competition between the AFM/FRM phases. Within this temperature range, the stability of theNéel vector decreases while the occurrence of the FRM moment becomes more prevalent. This destabilizes the axial anisotropy along the c-axis due to the transition from the AFM phase to FRM phase. Therefore, the interplay between S- ($\parallel$ Néel vector) and P-polarized ($\perp$ Néel vector) reflectance enhances, resulting in the first sign change in Fig. 3(a). Between 43 and 46 K, the phase competition weakens and the Kerr rotations start to decrease, leading to another sign change.

APPENDIX D: METHODS FOR OBTAINING THE FIGURE OF DEMAGNETIZATION PROCESS OBSERVED IN FRM STATE OF $X = 0.125$

To further support the demagnetization process discussed from Fig. 4(a) of the main text, we present evidence in the form of a hysteresis curve measured by Kerr rotations (θ) and the changes in the Kerr rotation angles ($\Delta\theta$) of the field-cooled FRM state following pump excitations. Figure 7(a) displays negative (positive) Kerr rotations for the magnetic field applied along the $+c$ ($-c$)-axis. After cooling the sample to the FRM state by applying a field along the $+c$-axis, we observe positive change in Kerr rotations ($\Delta\theta$) for three different pump polarizations, Fig. 7(b). This positive change is associated with a decrease in the moment along the $+c$-axis, indicating demagnetization processes for any pump polarization. The relationship M/M_s in Fig. 4(a) is derived by $(\theta + \Delta\theta)/\theta$.

[1] E. Beaurepaire, J.-C. Merle, A. Daunois, and J.-Y. Bigot, Ultrafast Spin Dynamics in Ferromagnetic Nickel, Phys. Rev. Lett. **76**, 4250 (1996).

[2] A. Scholl, L. Baumgarten, R. Jacquemin, and W. Eberhardt, Ultrafast Spin Dynamics of Ferromagnetic Thin Films Observed by fs Spin-Resolved Two-Photon Photoemission, Phys. Rev. Lett. **79**, 5146 (1997).

[3] G. P. Zhang and W. Hübner, Laser-Induced Ultrafast Demagnetization in Ferromagnetic Metals, Phys. Rev. Lett. **85**, 3025 (2000).

[4] T. Kise, T. Ogasawara, M. Ashida, Y. Tomioka, Y. Tokura, and M. Kuwata-Gonokami, Ultrafast Spin Dynamics and Critical Behavior in Half-Metallic Ferromagnet: Sr_2FeMoO_6, Phys. Rev. Lett. **85**, 1986 (2000).

[5] T. Ogasawara, K. Ohgushi, Y. Tomioka, K. S. Takahashi, H. Okamoto, M. Kawasaki, and Y. Tokura, General Features of Photoinduced Spin Dynamics in Ferromagnetic and Ferrimagnetic Compounds, Phys. Rev. Lett. **94**, 087202 (2005).

[6] J. Wang, C. Sun, J. Kono, A. Oiwa, H. Munekata, L. Cywiński, and L. J. Sham, Ultrafast Quenching of Ferromagnetism in

InMnAs Induced by Intense Laser Irradiation, Phys. Rev. Lett. **95**, 167401 (2005).

[7] M. Cinchetti, M. Sánchez Albaneda, D. Hoffmann, T. Roth, J.-P. Wüstenberg, M. Krauß, O. Andreyev, H. C. Schneider, M. Bauer, and M. Aeschlimann, Spin-Flip Processes and Ultrafast Magnetization Dynamics in Co: Unifying the Microscopic and Macroscopic View of Femtosecond Magnetism, Phys. Rev. Lett. **97**, 177201 (2006).

[8] C. D. Stanciu, A. Tsukamoto, A. V. Kimel, F. Hansteen, A. Kirilyuk, A. Itoh, and T. Rasing, Subpicosecond Magnetization Reversal across Ferrimagnetic Compensation Points, Phys. Rev. Lett. **99**, 217204 (2007).

[9] C. Stamm, T. Kachel, N. Pontius, R. Mitzner, T. Quast, K. Holldack, S. Khan, C. Lupulescu, E. F. Aziz, M. Wietstruk *et al.*, Femtosecond modification of electron localization and transfer of angular momentum in nickel, Nat. Mater. **6**, 740 (2007).

[10] G. Malinowski, F. Dalla Longa, J. H. H. Rietjens, P. V. Paluskar, R. Huijink, H. J. M. Swagten, and B. Koopmans, Control of speed and efficiency of ultrafast demagnetization by direct transfer of spin angular momentum, Nat. Phys. **4**, 855 (2008).

[11] G. M. Müller, J. Walowski, M. Djordjevic, G.-X. Miao, A. Gupta, A. V. Ramos, K. Gehrke, V. Moshnyaga, K. Samwer, J. Schmalhorst *et al.*, Spin polarization in half-metals probed by femtosecond spin excitation, Nat. Mater. **8**, 56 (2009).

[12] B. Koopmans, G. Malinowski, F. Dalla Longa, D. Steiauf, M. Fähnle, T. Roth, M. Cinchetti, and M. Aeschlimann, Explaining the paradoxical diversity of ultrafast laser-induced demagnetization, Nat. Mater. **9**, 259 (2010).

[13] I. Radu, G. Woltersdorf, M. Kiessling, A. Melnikov, U. Bovensiepen, J.-U. Thiele, and C. H. Back, Laser-Induced Magnetization Dynamics of Lanthanide-Doped Permalloy Thin Films, Phys. Rev. Lett. **102**, 117201 (2009).

[14] M. Battiato, K. Carva, and P. M. Oppeneer, Superdiffusive Spin Transport as a Mechanism of Ultrafast Demagnetization, Phys. Rev. Lett. **105**, 027203 (2010).

[15] A. Melnikov, I. Razdolski, T. O. Wehling, E. T. Papaioannou, V. Roddatis, P. Fumagalli, O. Aktsipetrov, A. I. Lichtenstein, and U. Bovensiepen, Ultrafast Transport of Laser-Excited Spin-Polarized Carriers in Au/Fe/MgO(001), Phys. Rev. Lett. **107**, 076601 (2011).

[16] T. Roth, A. J. Schellekens, S. Alebrand, O. Schmitt, D. Steil, B. Koopmans, M. Cinchetti, and M. Aeschlimann, Temperature Dependence of Laser-Induced Demagnetization in Ni: A Key for Identifying the Underlying Mechanism, Phys. Rev. X **2**, 021006 (2012).

[17] A. Eschenlohr, M. Battiato, P. Maldonado, N. Pontius, T. Kachel, K. Holldack, R. Mitzner, A. Föhlisch, P. M. Oppeneer, and C. Stamm, Ultrafast spin transport as key to femtosecond demagnetization, Nat. Mater. **12**, 332 (2013).

[18] W. Töws and G. M. Pastor, Many-Body Theory of Ultrafast Demagnetization and Angular Momentum Transfer in Ferromagnetic Transition Metals, Phys. Rev. Lett. **115**, 217204 (2015).

[19] T. Tsuyama, S. Chakraverty, S. Macke, N. Pontius, C. Schüßler-Langeheine, H. Y. Hwang, Y. Tokura, and H. Wadati, Photoinduced Demagnetization and Insulator-to-Metal Transition in Ferromagnetic Insulating BaFeO₃ Thin Films, Phys. Rev. Lett. **116**, 256402 (2016).

[20] S. R. Tauchert, M. Volkov, D. Ehberger, D. Kazenwadel, M. Evers, H. Lange, A. Donges, A. Book, W. Kreuzpaintner, U. Nowak, and P. Baum, Polarized phonons carry angular momentum in ultrafast demagnetization, Nature (London) **602**, 73 (2022).

[21] G. Ju, J. Hohlfeld, B. Bergman, R. J. M. van de Veerdonk, O. N. Mryasov, J.-Y. Kim, X. Wu, D. Weller, and B. Koopmans, Ultrafast Generation of Ferromagnetic Order via a Laser-Induced Phase Transformation in FeRh Thin Films, Phys. Rev. Lett. **93**, 197403 (2004).

[22] Y. M. Sheu, Y. M. Chang, C. P. Chang, Y. H. Li, K. R. Babu, G. Y. Guo, T. Kurumaji, and Y. Tokura, Picosecond Creation of Switchable Optomagnets from a Polar Antiferromagnet with Giant Photoinduced Kerr Rotations, Phys. Rev. X **9**, 031038 (2019).

[23] G. Ju, A. V. Nurmikko, R. F. C. Farrow, R. F. Marks, M. J. Carey, and B. A. Gurney, Ultrafast Time Resolved Photoinduced Magnetization Rotation in a Ferromagnetic/Antiferromagnetic Exchange Coupled System, Phys. Rev. Lett. **82**, 3705 (1999).

[24] M. van Kampen, C. Jozsa, J. T. Kohlhepp, P. LeClair, L. Lagae, W. J. M. de Jonge, and B. Koopmans, All-Optical Probe of Coherent Spin Waves, Phys. Rev. Lett. **88**, 227201 (2002).

[25] A. V. Kimel, A. Kirilyuk, A. Tsvetkov, R. V. Pisarev, and T. Rasing, Laser-induced ultrafast spin reorientation in the antiferromagnet TmFeO₃, Nature (London) **429**, 850 (2004).

[26] A. V. Kimel, A. Kirilyuk, P. A. Usachev, R. V. Pisarev, A. M. Balbashov, and T. Rasing, Ultrafast non-thermal control of magnetization by instantaneous photomagnetic pulses, Nature (London) **435**, 655 (2005).

[27] F. Hansteen, A. Kimel, A. Kirilyuk, and T. Rasing, Femtosecond Photomagnetic Switching of Spins in Ferrimagnetic Garnet Films, Phys. Rev. Lett. **95**, 047402 (2005).

[28] D. M. Wang, Y. H. Ren, X. Liu, J. K. Furdyna, M. Grimsditch, and R. Merlin, Light-induced magnetic precession in (Ga,Mn)As slabs: Hybrid standing-wave Damon-Eshbach modes, Phys. Rev. B **75**, 233308 (2007).

[29] K. Yamaguchi, M. Nakajima, and T. Suemoto, Coherent Control of Spin Precession Motion with Impulsive Magnetic Fields of Half-Cycle Terahertz Radiation, Phys. Rev. Lett. **105**, 237201 (2010).

[30] T. Kampfrath, A. Sell, G. Klatt, A. Pashkin, S. Mährlein, T. Dekorsy, M. Wolf, M. Fiebig, A. Leitenstorfer, and R. Huber, Coherent terahertz control of antiferromagnetic spin waves, Nat. Photonics **5**, 31 (2011).

[31] Z. Jin, Z. Mics, G. Ma, Z. Cheng, M. Bonn, and D. Turchinovich, Single-pulse terahertz coherent control of spin resonance in the canted antiferromagnet YFeO₃, mediated by dielectric anisotropy, Phys. Rev. B **87**, 094422 (2013).

[32] S. Baierl, M. Hohenleutner, T. Kampfrath, A. K. Zvezdin, A. V. Kimel, R. Huber, and R. V. Mikhaylovskiy, Nonlinear spin control by terahertz-driven anisotropy fields, Nat. Photonics **10**, 715 (2016).

[33] J. Lu, X. Li, H. Y. Hwang, B. K. Ofori-Okai, T. Kurihara, T. Suemoto, and K. A. Nelson, Coherent Two-Dimensional Terahertz Magnetic Resonance Spectroscopy of Collective Spin Waves, Phys. Rev. Lett. **118**, 207204 (2017).

[34] M. Hudl, M. d'Aquino, M. Pancaldi, S.-H. Yang, M. G. Samant, S. S. P. Parkin, H. A. Dürr, C. Serpico, M. C. Hoffmann, and

S. Bonetti, Nonlinear Magnetization Dynamics Driven by Strong Terahertz Fields, Phys. Rev. Lett. **123**, 197204 (2019).

[35] A. Kirilyuk, A. V. Kimel, and T. Rasing, Ultrafast optical manipulation of magnetic order, Rev. Mod. Phys. **82**, 2731 (2010).

[36] J. Walowski and M. Münzenberg, Perspective: Ultrafast magnetism and THz spintronics, J. Appl. Phys. **120**, 140901 (2016).

[37] R. V. Mikhaylovskiy, T. J. Huisman, V. A. Gavrichkov, S. I. Polukeev, S. G. Ovchinnikov, D. Afanasiev, R. V. Pisarev, T. Rasing, and A. V. Kimel, Resonant Pumping of $d-d$ Crystal Field Electronic Transitions as a Mechanism of Ultrafast Optical Control of the Exchange Interactions in Iron Oxides, Phys. Rev. Lett. **125**, 157201 (2020).

[38] S. Toyoda, M. Fiebig, T. hisa Arima, Y. Tokura, and N. Ogawa, Nonreciprocal second harmonic generation in a magnetoelectric material, Sci. Adv. **7**, eabe2793 (2021).

[39] Y. M. Sheu, S. A. Trugman, Y.-S. Park, S. Lee, H. T. Yi, S.-W. Cheong, Q. X. Jia, A. J. Taylor, and R. P. Prasankumar, Ultrafast carrier dynamics and radiative recombination in multiferroic BiFeO$_3$, Appl. Phys. Lett. **100**, 242904 (2012).

[40] T. Kurumaji, S. Ishiwata, and Y. Tokura, Doping-tunable ferrimagnetic phase with large linear magnetoelectric effect in a polar magnet Fe$_2$Mo$_3$O$_8$, Phys. Rev. X **5**, 031034 (2015).

[41] This is based on our observation of domain sizes versus doping concentrations. For doping concentration 12.5%, $x = 0.125$, the domain size is largest, then decreases for $x = 0.25$, and eventually becomes unmeasurable for $x = 0.4$ due to our optical resolution of ~ 0.5 μm. The domain image for $x = 0.25$ is shown in Fig. 6(b) in Appendix B.

[42] The spin-lattice relaxation time depends on spin-specific heat [43], which in turn varies with temperature. Through our ananlysis, we determine that the two-exponential fitting method, with the fewest free parameters, provides the most effective approach across all the experimental temperature ranges to account for the changes in spin-specific heat during the spin-lattice relaxation.

[43] R. D. Averitt, A. I. Lobad, C. Kwon, S. A. Trugman, V. K. Thorsmølle, and A. J. Taylor, Ultrafast Conductivity Dynamics in Colossal Magnetoresistance Manganites, Phys. Rev. Lett. **87**, 017401 (2001).